THE ANATOMICAL RECORD 252:311–324 (1998)

Regeneration and Myogenic Cell Proliferation Correlate With Taurine Levels in Dystrophin- and MyoD-Deficient Muscles

LAURA M. McINTOSH,[1] KERRYN L.GARRETT,[2] LYNN MEGENEY,[3] MICHAEL A. RUDNICKI,[3] AND JUDY E. ANDERSON[4]*

[1]Institute for Biodiagnostics, National Research Council of Canada, Winnipeg, Manitoba, Canada
[2]Lions Eye Institute, Queen Elizabeth II Medical Centre, Perth Western Australia, Australia
[3]MOBIX- (Institute for Molecular Biology & Biotechnology), McMaster University, Hamilton, Ontario, Canada
[4]Department of Human Anatomy and Cell Science, University of Manitoba, Winnipeg, Canada

ABSTRACT

This study coupled proton magnetic resonance spectroscopy (^{1}H-NMR) and in situ hybridization plus autoradiography in a novel examination of different phenotypes of adult myogenesis that arise from genetic disruptions in mice. Study of muscle extracts from normal and dystrophin-deficient *mdx* limb and diaphragm muscles confirmed our previous findings linking taurine and muscle regeneration at the peak of damage and repair. ^{1}H-NMR distinguished biochemical differences in regenerating muscles that were consistent with the extent of repair in three strains: *mdx* dystrophic mice; MyoD(-/-) mice that lack expression of the early myogenic regulatory gene MyoD; and a double-mutant *mdx*:MyoD(-/-) strain lacking expression of both MyoD and dystrophin. We tested the hypothesis that differences in spectra according to genotype and the regeneration phenotype are related specifically to proliferation by committed myogenic precursor cells. ^{1}H-NMR distinguished the three mutant strains: Taurine was highest in *mdx* muscles, with the phenotype of most effective regeneration; lowest in MyoD(-/-) muscles, with the least effective formation of new muscle in repair, as reported previously; and intermediate in double-mutant muscles, now reported to show an intermediate repair phenotype. The early and late muscle precursors (mpcs) expressing myf5 and myogenin were examined for proliferation. Eighteen percent of *mdx* myf5-positive mpcs were proliferative, whereas myf5-positive mpcs did not proliferate in regenerating muscles that lacked MyoD expression. By contrast, whereas 30% of myogenin-positive mpcs were proliferative in *mdx* muscles, almost none were proliferative in MyoD(-/-) muscles, and 12% were proliferative in double-mutant muscles. Therefore, the extent of accumulated structural regeneration, taurine levels, and proliferation of late mpc (expressing myogenin) were congruent across genotypes. Proliferation by early mpc (expressing myf5) was inhibited by the lack of MyoD expression during muscle regeneration. These studies indicate the potential for ^{1}H-NMR monitoring of muscle status in disease, regeneration, and treatment. Anat. Rec. 252:311–324, 1998.

Key word: proton magnetic resonance spectroscopy; in situ hybridization; *mdx* dystrophy; MyoD; myogenin; myf5; diaphragm; cardiomyopathy

Grant sponsor: Children's Hospital Research Foundation; Grant sponsor: Muscular Dystrophy Association; Grant sponsor: Medical Research Council of Canada; Grant sponsor: National Cancer Institute.

*Correspondence to: Dr. Judy Anderson, Department of Human Anatomy and Cell Science, University of Manitoba, 730 William Avenue, Winnipeg, Canada R3E 0W3.
E-mail: janders@ms.umanitoba.ca

Received 17 March 1998; Accepted 20 May 1998

The ability to detect the phenotype of disease and the extent of regeneration in a muscle would greatly assist treatments of muscle disease that, along with drugs or myoblast transfer, are aimed at new muscle formation. This study bridged two very distinct fields of investigation: proton magnetic resonance spectroscopy (^{1}H-NMR) and gene expression, particularly myogenic regulatory gene (MRF) expression in regeneration of skeletal muscle. ^{1}H-NMR is available in clinical magnetic resonance imaging (MRI) facilities and ultimately could be a noninvasive diagnostic modality for such purposes. The study of metabolism in normal and diseased tissue can apply ^{1}H-NMR, because spectra are direct indicators of tissue biochemistry (Peeling and Sutherland, 1992; Kuesel et al., 1994; Rutter et al., 1995; McIntosh et al., 1998). Because the levels of some endogenous metabolites are affected by disease, it is proposed that NMR spectroscopy can monitor biochemical changes that correlate with disease states and tissue phenotypes, similar to our initial findings that correlated central nucleation in regeneration of muscle with levels of particular spectral peaks (McIntosh et al., 1998). In situ hybridization and autoradiography are well-established techniques that are used to determine cell identity and proliferation, respectively, as direct indicators of a phenotype. In this study, we have chosen to use ^{1}H-NMR spectroscopy in tandem with detailed histology, in situ hybridization, and autoradiography to examine muscle regeneration in three conditions, namely, genotypic changes to muscle, progression of dystrophic disease, and imposed injury.

The expression of the four MRFs, myf5, MyoD, myogenin, and MRF4, in two developmentally redundant pairs is thought to control the early commitment or determination of the skeletal muscle lineage (involving MyoD and myf5 expression) and the later differentiation of muscle precursors (mpcs) and myofibers (involving myogenin and MRF4 expression) during myogenesis (Weintraub et al., 1991; Megeney and Rudnicki, 1995; Rudnicki and Jaenisch, 1995). The distinctive roles of the MRFs in muscle regeneration are less clear. For example, mice that lack expression of MyoD develop overtly normal skeletal muscle (Rudnicki et al., 1992) but demonstrate a dramatically reduced capacity for regeneration after an imposed injury (Megeney et al., 1996). Limb muscles of mice that lack both dystrophin and MyoD [*mdx*:MyoD(-/-), double mutants] exhibit a more severe myopathy than limb muscles of *mdx* mice (that do express MyoD; Megeney et al., 1996). Although the absence of MyoD does not appear to affect the development of muscle, that deficiency is deleterious to muscle regeneration and accentuates disease progression in *mdx* dystrophy. However, the precise mechanism(s) underlying those effects of MyoD deficiency is not clear.

The *mdx* mouse is a genetic homologue to human Duchenne muscular dystrophy (DMD). Skeletal muscle cells in *mdx* mice display segmental myofiber damage due to a lack of dystrophin and a decrease in dystrophin-associated glycoproteins in the subsarcolemmal cytoskeleton (Matsumura and Campbell, 1994; Mizuno et al., 1994). Regeneration after the onset of dystrophy is very successful in *mdx* limb muscles (Anderson et al., 1987; 1988). However, the *mdx* diaphragm is affected much more severely by dystrophy (Stedman et al., 1991; Dupont-Versteegden and McCarter, 1992), which, as we recently reported, is worse in crural regions than in costal regions of the diaphragm (Anderson et al., 1998).

Our previous ^{1}H-NMR work on tissue biopsies (ex vivo samples) of limb and diaphragm muscles demonstrated that ^{1}H-NMR spectroscopy discriminates the two different muscles (limb versus diaphragm) as well as distinguishing normal muscle from *mdx* muscle (McIntosh et al., 1998). Ex vivo ^{1}H-NMR also distinguished three distinct stages of dystrophy in *mdx* mice and between groups of muscles collected from *mdx* mice under different glucocorticoid treatments (McIntosh et al., 1998). In addition, fiber central nucleation, which is a key histologic feature of muscle regeneration, was correlated highly and significantly to concentrations of certain resonance peaks, including taurine.

Although a large degree of tissue integrity is maintained in ex vivo samples, ^{1}H-NMR spectra from ex vivo tissues typically have wide, overlapping peaks and a large component from lipids that obscures many smaller resonance signals from amino acids. Because broad peaks likely are contributed by multiple metabolites, the integrated area or intensity of such peaks is only a general indicator of the dynamic metabolic state of a tissue. In contrast, the analysis of acid extracts of tissues with high-resolution ^{1}H-NMR allows much more precise determination of the concentrations of many water-soluble, low-molecular-weight metabolites, aids in assignment of metabolites, and can be used to verify ex vivo spectroscopic results without tissue histology. At present, there are no detailed reports of extracts from *mdx* mice, especially in the amino acid-rich region of the spectrum, that show consistent muscle-specific changes in disease and after treatment.

In this study, we combined two very distinct methods in a novel examination of muscle regeneration. ^{1}H-NMR spectroscopy of perchloric acid extracts from normal and *mdx* limb and diaphragm muscles (part I) were investigated in order to confirm our previous ex vivo study (McIntosh et al., 1998) and to elucidate further the metabolism of muscle during the peak period of damage. Part II paired investigations of metabolism with studies of proliferation and differentiation (by using autoradiography and in situ hybridization) during muscle repair in three mutant strains [*mdx*, MyoD(-/-), and *mdx*:MyoD(-/-) double mutants] to test the hypothesis that differences in dystrophin and MyoD expression affect myogenic cell proliferation, correlate with the extent of muscle regeneration, and are visible by using ^{1}H-NMR.

MATERIALS AND METHODS

Metabolites in Extracts of Skeletal Muscles (Part I)

Animals. Normal control (C57Bl/10ScSn) and *mdx* mice were maintained and housed according to the Canadian Council of Animal Care (CCAC) at the University of Manitoba Animal Care Facility. Control (n = 6) and *mdx* (n = 5) mice, 5 weeks of age, were killed by cervical dislocation under anaesthetic, and the tibialis anterior (TA) and diaphragm (DIA) muscles were collected.

Tissue preparation. Muscles were removed rapidly, placed in preweighed vials, frozen in liquid nitrogen, reweighed, and stored at -70°C. Perchloric acid extraction was performed according to published methods (Peeling and Sutherland, 1992, 1993). Briefly, muscles were homogenized twice with cold 0.3 M perchloric acid (1 ml per 100 mg tissue), and the supernatants were collected and neutralized with cold 1.5 M KOH to pH 7.0 (±0.2). After

lyophilizing, 1 ml of D_2O was added to the dry extracts, which were then brought to pH 7.25 (±0.2) with NaOD and DCl, using deuterium (D) to eliminate the hydrogen signal in aqueous solutions. Samples were lyophilized again and stored. One day before acquiring NMR spectra, 0.60 ml of 1.5 mM sodium 3-trimethysilylpropionate (TSP; a chemical shift reference) in D_2O was added to the dry extract, the pH was checked, and the sample was pipetted into a clean 5-mm NMR tube. One to two samples were prepared for each muscle.

NMR. ^{1}H-NMR spectra were obtained at 25°C with an AMX500 Bruker Spectrospin spectrometer (Frankfurt, Germany) locked to the D_2O resonance. For each sample, 160 free induction decays (FIDs) were accumulated in 16 K of memory by using a spectral width of 5,050.5 Hz (acquisition time of 1.62 sec). Fourier transformation using exponential multiplication (LB = 0.30 Hz) was applied to give the NMR spectrum. Two orders of zero filling were applied.

Peak assignment to the metabolites of interest in the muscle extract spectra were made on the basis of chemical shift values from the literature for extracts of skeletal muscle (Arus and Barany, 1986; Venkatasubramanian et al., 1986), lymphocytes (Sze and Jardetzky, 1990, 1994), colon (Moreno and Arus, 1996), and pure compounds and had the expected pH behavior and J-couplings. An integration routine using *xspec* software (version 2.0.7, Bruker) was used to determine the areas under the peaks (parts per million; ppm) assigned to lactate (1.33 and 4.11), alanine (1.47), glutamate (2.35), succinate (2.41), glutamine (2.45), creatines (3.04 and 3.93), carnitine (3.23), taurine (3.26 and 3.42), glycine (3.56), and glucose (4.65). The concentration (µmol/g) of each assigned metabolite was determined by comparing the integrated intensity of the metabolite with the TSP signal for that sample, correcting for the number of protons contributing to the particular peak and for the tissue weight (wet weight) of the sample (Peeling and Sutherland, 1992, 1993). Statistical comparisons (NWA Statpak, Portland OR) were performed by using unpaired t-tests, and a probability of $P < 0.05$ was used to reject the null hypothesis.

Metabolites (Part IIA) and Myogenic Cell Proliferation (Part IIB) by ^{1}H-NMR, In Situ Hybridization, and Autoradiography

Animals. *Mdx*, MyoD(-/-) (Rudnicki et al., 1992), and homozygous double-mutant *mdx*:MyoD(-/-) mice (Megeney et al., 1996) were used in these experiments, and genotypes were confirmed by using tail DNA and Southern blotting (Megeney et al., 1996). Mice from the three strains were bred in the McMaster University barrier facility according to guidelines of the CCAC and were transported to the University of Manitoba. At 4 months of age, each animal received a crush injury to the right TA muscle under ketamine:xylazine anesthesia, exactly as reported previously (McIntosh et al., 1994). Animals were allowed to recover for 4 days. Three days after injury, mice received an intraperitoneal injection of ^{3}H-thymidine (2 µCi/g body weight; Amersham Life Sciences, Mississauga, ON; McIntosh and Anderson, 1995). Twenty-four hours later, mice were killed under anesthesia.

Tissue preparation. The left (uncrushed) TA (LTA), the regenerating right (uncrushed) TA (RTA), the DIA muscles, and the heart were dissected rapidly from mice. One half of each muscle (with the exception of heart tissue) was placed individually in PBS/D_2O, pH 7.4, and snap frozen in liquid nitrogen for NMR spectroscopy. The other halves were embedded in Tissue Tek Optimal Cutting Temperature (OCT; Miles Scientific, Inc., Elkhart, IN) compound and frozen for in situ hybridization/autoradiography.

NMR (Part IIA)

Samples were stored at -80°C. Muscles were thawed and positioned in an NMR tube (Kuesel et al., 1992), and ^{1}H NMR spectra were acquired on an AMX500 Bruker Spectrospin Spectrometer, exactly as described (McIntosh et al., 1998). Resonances in the ex vivo muscle spectra were assigned as reported (McIntosh et al., 1998). Peak areas and heights were determined for six bands (*xspec* version 2.0.7; Bruker), which are due mainly to creatines (peaks 1 and 4), taurine (peaks 2 and 3), lipids (peak 5), and amino acids (peak 6). Peak areas and heights were normalized to tissue mass and to the paraminobenzoic acid (PABA) reference peak (McIntosh et al., 1998). Ratios of all combinations of areas and heights were also determined on each spectrum, because the ratio of two peak heights or areas allows peaks to act as internal standards for the variations due to mass in individual samples. Data were decoded, and the mean ± standard error of the mean (SEM) was determined for each muscle group (LTA, RTA, and DIA) and for each genotype (*mdx*, MyoD(-/-), and double-mutant mice) and was tested for significant effects by using a two-way, repeated-measures analysis of variance (ANOVA; Statpak; NWA). Specific t-tests were then performed on the peaks that were found significant by two-way ANOVA in order to determine selected differences of particular interest. A probability of $P < 0.05$ was used. Following acquisition of spectra, samples were blotted, weighed, and fixed in 10% Formalin for histology to check tissue character and to be certain that no grossly visible fat accumulations or tendons were present.

In Situ Hybridization and Autoradiography (Part IIB)

Cryosections (6 µm thick) were collected onto silanated slides. Studies of tissue integrity (LTA, DIA, heart) and muscle regeneration (RTA) were made on hematoxylin and eosin (H&E)-stained sections. Two serial slides from RTA and LTA muscles were processed by using the identical in situ hybridization protocols in order to localize mRNAs of the early and late MRFs, myf5 and myogenin, respectively, in muscle precursors and myotubes (Garrett and Anderson, 1995). After the in situ protocol, slides were processed for autoradiography as described previously (McIntosh and Anderson, 1995). The following categories of mononuclear cells were counted in sections of regenerating muscles: 1) MRF-positive (MRF+) cells (myf5+ or myogenin+ cells), 2) mononuclear cells overlaid with silver grains, and 3) mononuclear cells showing MRF+ staining and silver grains. A total of 300–600 cells per section were counted over four to six fields at a magnification of ×400 in RTA muscles in order to quantify MRF+ cell proliferation during regeneration. The subset of mononuclear cells that contained both nuclei overlaid with silver grains and the cytoplasmic digoxigenin signal for either myf5 or myogenin mRNA was expressed as the proliferative proportion of the myf5+ or myogenin+ muscle precursor cells, respectively. The proliferative proportions of myf5+ and myo-

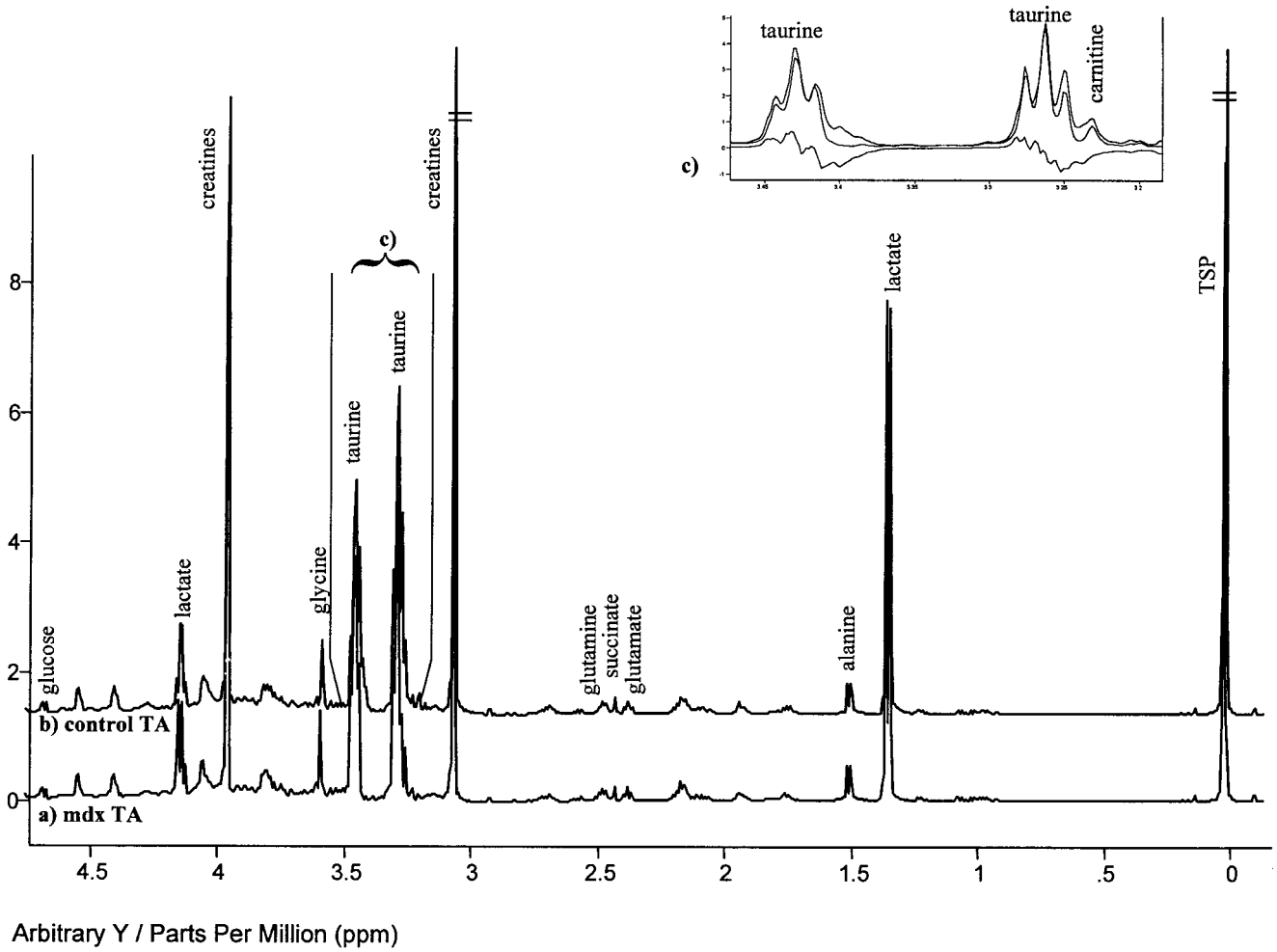

Fig. 1. Mean proton magnetic resonance spectroscopy (^{1}H-NMR) spectra of perchloric acid extracts of tibialis anterior (TA) samples. The peaks of interest are labeled. Lactate resonates at 1.33 ppm (CH_3 doublet) and 4.11 ppm (CH quartet), alanine resonates at 1.47 ppm (CH_3 doublet), glutamate resonates at 2.35 ppm (CH_2 triplet of doublets), succinate resonates at 2.41 ppm (CH_2 singlet), glutamine resonates at 2.45 ppm (CH_2 complex), creatines resonate at 3.04 ppm (CH_3 singlet) and 3.93 ppm (CH_2 singlet), carnitine resonates at 3.23 ppm (N-CH_3 singlet), taurine resonates at 3.26 ppm (S-CH_2 triplet) and 3.42 ppm (N-CH_2 triplet), glycine resonates at 3.56 ppm (CH_2 singlet), and glucose resonates at 4.65 ppm (CH doublet). TSP is the reference peak and is normalized to the same value in all spectra. **a:** Averaged *mdx* TA spectrum. **b:** Averaged normal control TA spectrum. **c:** An enlarged region between 3.15 ppm and 3.5 ppm showing taurine and carnitine peaks where the top spectrum is the average of control TA spectra, the middle spectrum is the average of *mdx* TA spectra, and the bottom trace represents the difference between the two average spectra (*mdx* minus control). In this difference spectrum, the negative peaks indicate lower amounts, and positive peaks indicate higher amounts of metabolite in *mdx* spectra compared with control. Although the average spectra appear similar, the amounts of taurine and carnitine are lower in *mdx* than in control TA muscles.

genin+ cells in each group (*mdx*, MyoD(-/-), and double-mutant mice) were calculated (mean ± SD), and differences among regenerating (RTA) muscles from the three strains and between myf5+ and myogenin+ cells were determined by using a two-way, repeated-measures ANOVA (NWA). A probability of $P < 0.05$ was used to determine significance.

RESULTS

NMR of Control and *mdx* Muscle Extracts (Part I)

Proton NMR spectroscopy of perchloric acid extracts of control and *mdx* muscles was performed to confirm the results from our previous ex vivo NMR study (McIntosh et al., 1998) and for a detailed study of the metabolism in normal and dystrophic muscle. NMR spectra of muscle extracts showed narrow, distinct peaks on a flat baseline. Peak assignments are labelled in Figures 1 and 2 (see legends), which show average spectra from normal and *mdx* groups of TA (Fig. 1) and DIA (Fig. 2) extracts. No extra or different peaks are present in spectra of *mdx* muscle extracts compared with normal muscle spectra. However, certain peaks have consistently different areas in *mdx* spectra versus control spectra, as shown in examples of difference spectra (Figs. 1c, 2c).

Table 1 shows the concentration of the metabolites of interest in this study. Peaks attributed to carnitine and taurine were significantly lower in *mdx* TA extracts com-

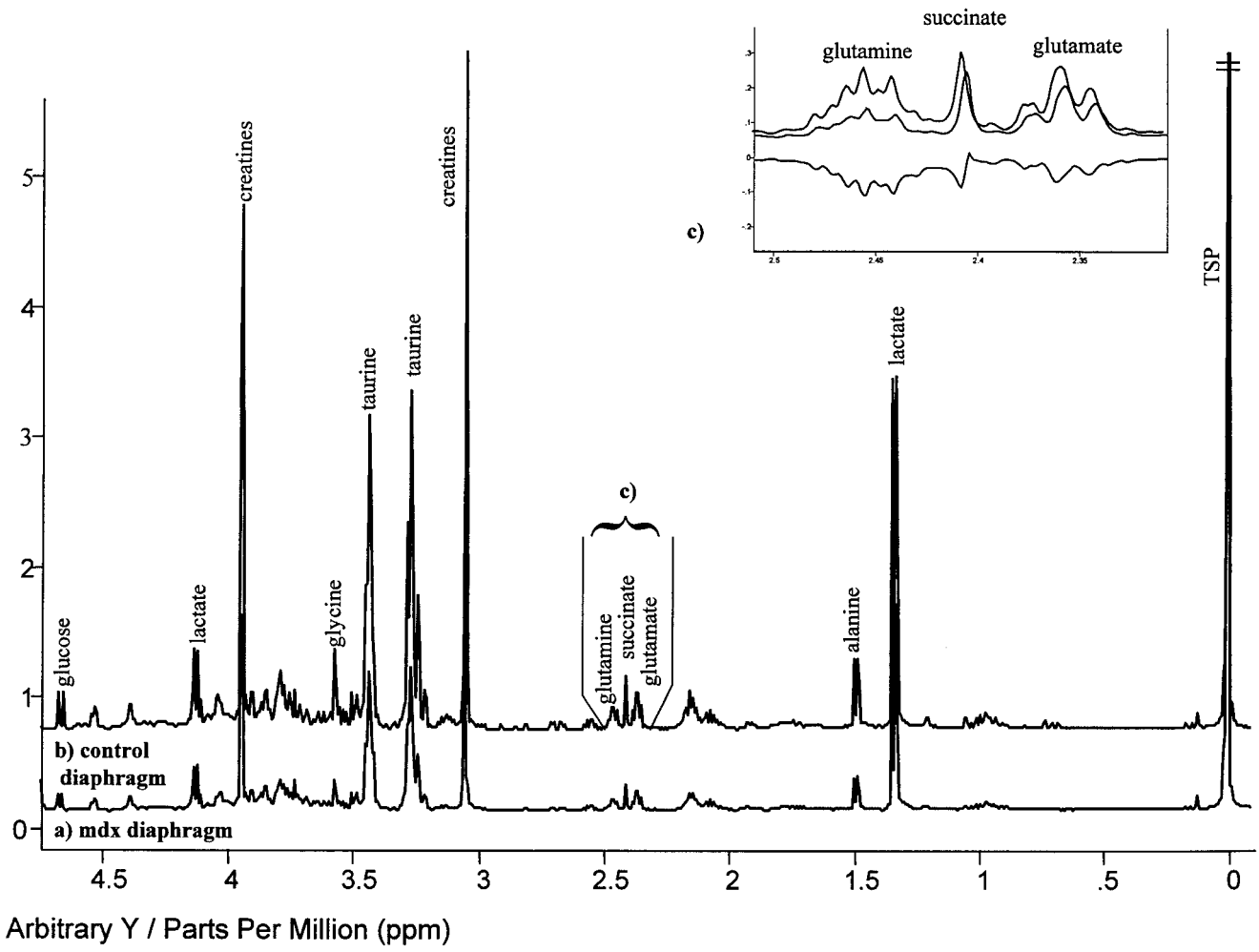

Fig. 2. Mean ^{1}H-NMR spectra of perchloric acid extracts of diaphragm (DIA) samples. The peaks of interest are labeled as in Figure 1. TSP is the reference peak and is normalized to the same value in all spectra. **a:** Averaged *mdx* DIA spectrum. **b:** Averaged normal control DIA spectrum. **c:** An enlarged region between 2.3 ppm and 2.5 ppm showing glutamate, succinate, and glutamine peaks where the top spectrum is the average of control DIA spectra, the middle spectrum is the average of *mdx* DIA spectra, and the bottom trace represents the difference between the two average spectra (*mdx* minus control). Therefore, in this difference spectrum, negative peaks represent lower amounts of metabolite in *mdx* spectra compared with control, whereas positive peaks represent higher amounts of metabolite in *mdx* spectra compared with control. Although the mean spectra appear very similar, the amounts of glutamate, succinate and glutamine are lower in *mdx* than in control DIA muscles.

pared with control TA extracts. Alanine, glutamate, succinate, creatine, taurine, and glycine peaks were significantly lower in *mdx* extracts compared with normal DIA extracts. In addition, lactate, glutamine, creatines, taurine, and glycine levels were lower in DIA than in TA, whereas glutamate, succinate, and glucose levels were higher in DIA than in TA. The extracts allowed better separation of metabolites and resolved additional peaks than was possible by peak assignments of ex vivo spectra, whereas the difference in the taurine resonances reproduced the earlier findings.

Ex Vivo NMR of *mdx*, MyoD (-/-), and Double-Mutant Muscles (Part IIA)

Previous studies (Megeney et al., 1996) showed that muscle regeneration was decreased in mice that lacked MyoD expression despite the overtly normal development of muscles in that mutant. Proton NMR spectroscopy of ex vivo samples from the three mutant strains was performed to determine whether ^{1}H-NMR could monitor metabolic changes in muscle regeneration that occur in relation to differences in genotype of muscle. General observation of spectra (Fig. 3) shows that the profiles are similar among TAs and DIAs, but TA and DIA spectra differ in appearance of the lipid -CH_2 and lactate resonances (peaks 5 and 6), as noted previously for *mdx* mice and the normal parent strain (McIntosh et al., 1998).

Typically, peaks that contain resonances from proton bonds in taurine (peaks 2 and 3), carnitine (peak 3), and creatines (peak 4) were higher in spectra from *mdx* LTA than MyoD(-/-) LTA muscles. The same peaks were also significantly higher in regenerating muscles (*mdx* LTA and all RTA muscles) than in nonregenerating MyoD(-/-) LTA and in poorly regenerating DIA muscles of *mdx* and double-mutant mice. Peaks assigned to lipid and lactate (peaks 5 and 6) were lower in regenerating muscles.

TABLE 1. Concentrations (Mean ± SEM; μmol/g) of Metabolites of Interest From Proton Magnetic Resonance Spectroscopy Spectra of Perchloric Acid Extracts of Tibialis Anterior and Diaphragm Muscles From 5-Week-Old Control and *mdx* Mice (part I)

Metabolite	Control TA (n = 12)	*Mdx* TA (n = 10)	Control DIA (n = 6)	*Mdx* DIA (n = 5)
Lactate	1.43 ± 0.17	1.54 ± 0.21	1.07 ± 0.17	0.80 ± 0.06
Alanine	0.13 ± 0.01	0.14 ± 0.01	0.19 ± 0.01	0.15 ± 0.02 (P = 0.05)**
Glutamate	0.10 ± 0.01	0.10 ± 0.01	0.24 ± 0.02	0.19 ± 0.01 (P = 0.04)**
Succinate	0.04 ± 0.005	0.03 ± 0.005	0.14 ± 0.03	0.07 ± 0.01 (P = 0.04)**
Glutamine	0.13 ± 0.01	0.12 ± 0.01	0.16 ± 0.01	0.14 ± 0.01
Creatines	1.72 ± 0.13	1.50 ± 0.13	0.94 ± 0.05	0.60 ± 0.05 (P = 0.003)**
Carnitine	0.06 ± 0.003	0.05 ± 0.005 (P = 0.02)*	0.08 ± 0.005	0.06 ± 0.009
Taurine	2.61 ± 0.18	2.17 ± 0.20 (P = 0.05)*	1.85 ± 0.08	1.33 ± 0.14 (P = 0.03)**
Glycine	0.29 ± 0.02	0.29 ± 0.03	0.16 ± 0.02	0.12 ± 0.01 (P = 0.05)**
Glucose	0.11 ± 0.02	0.11 ± 0.02	0.26 ± 0.03	0.21 ± 0.03

*Significantly different from control limb.
**Significantly different from control diaphragm (DIA). TA, tibialis anterior.

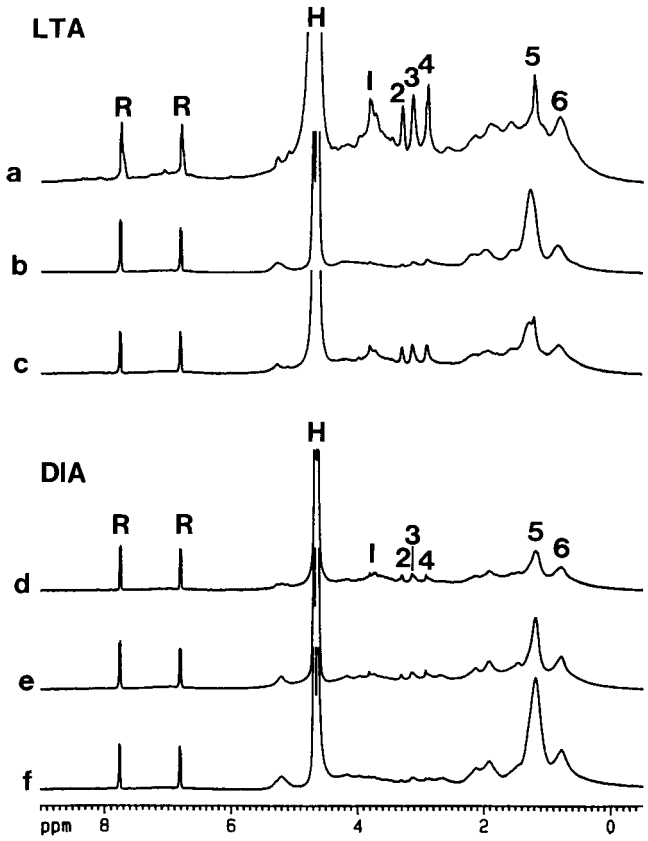

Fig. 3. Typical spectra of left (uncrushed) TA (LTA; top) and DIA (bottom) from *mdx* (a,d), MyoD(-/-) (b,e), and double-mutant (DM) mice (c,f). The reference paraminobenzoic acid (PABA) peak (R) is normalized to the same value in all spectra. The water peak (H) is shown. Peaks 1–6 are assigned as follows: creatines at 3.9 ppm (peak 1) and 3.0 ppm (peak 4), taurine at 3.4 ppm (peak 2) and 3.2 ppm (peak 3; with contributions from cholines and carnitine), lipids and lactate at 1.3 ppm (peak 5), and lipids and amino acids at 0.9 ppm (peak 6). **a–c:** Creatine, taurine, and choline peaks (1–4) are largest in the spectrum from *mdx* LTA muscle (a) and smallest in the spectrum of MyoD(-/-) LTA (b). In the spectrum from double-mutant LTA (c), peaks 1–4 are intermediate in height between *mdx* and MyoD(-/-) spectra. **d–f:** In DIA, peaks 5 and 6 dominate the spectra. Peaks 1–4 are smaller in DIA than in LTA muscles and are present with similar relative differences between *mdx* (d), MyoD(-/-) (e), and double-mutant DIA (f).

Generally, peak heights for peaks 1–4 in double-mutant and MyoD(-/-) muscles were very similar for LTA and RTA tissues, likely due to the relatively poor regeneration from dystrophy (in double mutants) or from injury [in MyoD(-/-) and double-mutant mice]. In *mdx* mice, injury to RTA induced substantially more regeneration relative to dystrophy in the LTA, as reported previously (McIntosh et al., 1994; Pernitsky et al., 1996).

Analysis of peak areas followed the same trends as for peak heights: Peaks 1–4 were each significantly greater in *mdx* muscles than in double-mutant or MyoD(-/-) muscles. The ratio of peak areas 3/1 (taurine:creatine) was significantly larger in *mdx* mice than in the other two strains that lacked MyoD expression. Heights, areas, and ratios for the double-mutant spectra were always intermediate between values for *mdx* and MyoD(-/-) muscle spectra.

Regeneration, In Situ Hybridization, and Autoradiography (part IIB)

The purpose of these studies was to determine whether aspects of proliferation and myogenic differentiation might account for differences in regeneration by muscles of different phenotypes and whether the level of myogenic cell proliferation is related to biochemical changes that are visualized by ^{1}H-NMR. The phenotype of *mdx* muscles (LTA, DIA, and RTA) has been reported elsewhere (Dangain and Vrbova, 1984; McIntosh et al., 1994; Anderson et al., 1987, 1998). MyoD(-/-) LTA and DIA muscles were largely normal, as reported previously (Megeney et al., 1996).

In double-mutant muscles, the prevalence of focal lesions characteristic of dystrophy was dramatically greater, and focal muscle regeneration was less apparent in LTA (Fig. 4) compared with those from *mdx* mice and in DIA (Fig. 5) and cardiac (Fig. 6) muscles compared with those from *mdx* and MyoD(-/-) mice. DIA muscles from double mutants were markedly thinner than DIA from the other two strains and were always grossly streaked by calcified fiber bundles radiating toward the costal margins from the central tendon. Microscopically, double-mutant DIA contained far fewer fibers in a cross-sectional plane than were seen in double-mutant or *mdx* DIA (Fig. 5c). Double-mutant cardiac tissues contained large lesions that were visible grossly in epicardial, endocardial, and interventricular regions. Severe calcification, cardiomyocyte necrosis,

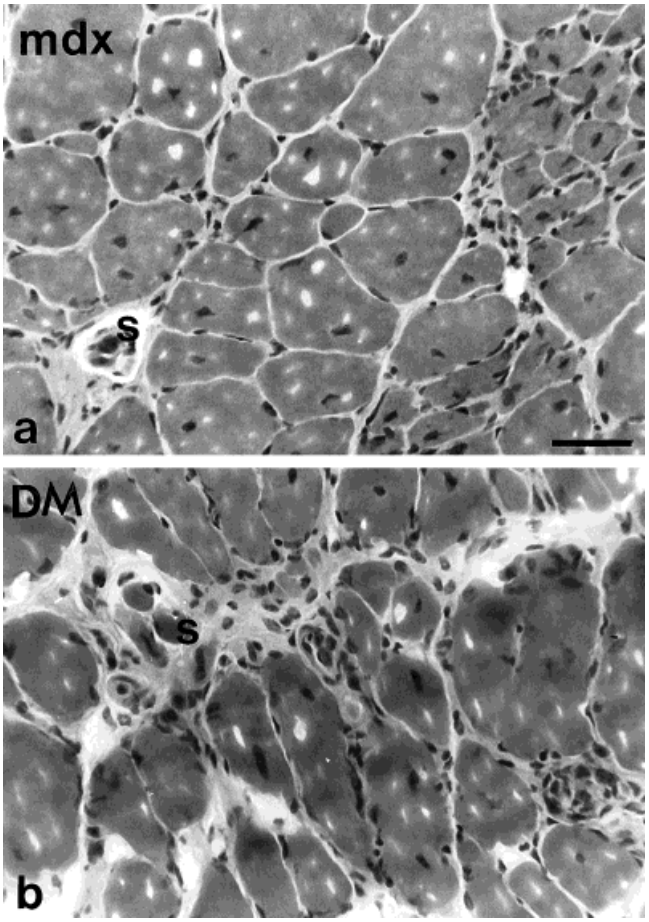

Fig. 4. Light photomicrographs of *mdx* (**a**) and double-mutant (**b**) LTA muscles. Many fibers contain central or eccentric nuclei, indicating the moderate (a) and high (b) prevalence of previous dystrophic damage to fibers in each field. Double-mutant muscles also showed disrupted fascicles and more small-diameter fibers, consistent with the increased severity of dystrophy compared with mdx LTA. Muscle spindles (s) are indicated (magnification ×240). Scale bar = 50 μm.

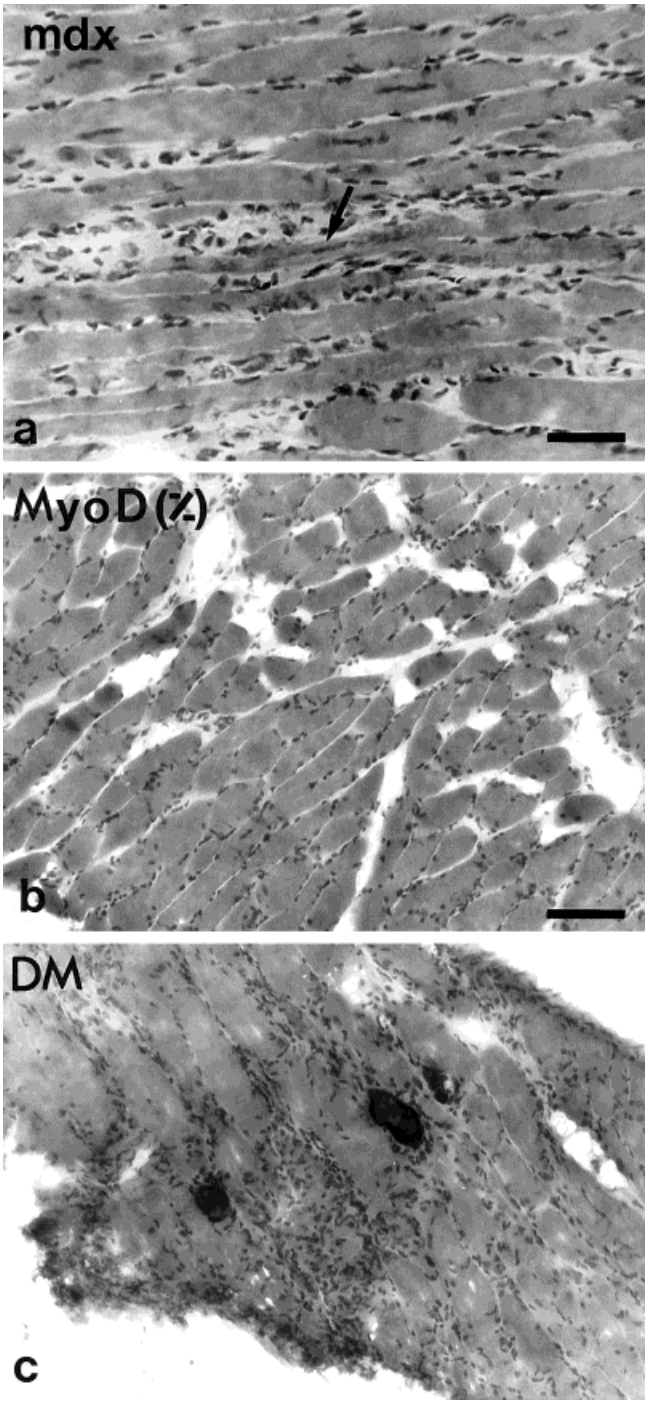

Fig. 5. DIA muscles from *mdx* (a), MyoD(-/-) (b), and double-mutant (c) mice. **a:** *mdx* DIA in this longitudinal section shows regions of mononuclear cell infiltration, necrotic fiber segments, and new myotubes (arrow) interspersed with undamaged fibers (magnification ×240). **b:** DIA of the MyoD(-/-) mouse seen in cross section showing fascicles of normal fibers containing only occasional central nuclei (magnification ×120). **c:** DIA of the double-mutant mouse, seen here in an oblique section, is grossly thinner than DIA from MyoD(-/-) or *mdx* mice. Frequent calcification, fiber damage, inflammation, and many small myotubes are also visible in the section (magnification ×120). Scale bars = 50 μm in a, 100 μm in b (also applies to c).

mononuclear cell infiltration, and fibrosis of older lesions were observed in sections (Fig. 6c) and were often transmural. These histologic data now greatly extend the previous indication (Megeney et al., 1996) that the absence of both MyoD and dystrophin in muscles of double-mutant mice is associated with severe myopathy in limb, diaphragm, and cardiac muscles.

Regeneration of *mdx* and MyoD(-/-) muscle was reported previously (Megeney et al., 1996). Briefly, in *mdx* RTAs (Fig. 7a,b), large and elongated myotubes that contain many nuclei nearly fill the region between surviving muscle (outside the region of injury) and the crushed region. Many mpcs (expressing MRFs; not shown here) were observed angled toward the ends and sides of surviving fiber segments (Fig. 7b). RTA muscles from MyoD(-/-) mice contained far fewer, smaller myotubes that had fewer internal nuclei compared with *mdx* myotubes at the same recovery time, and many mononuclear cells were present in the large necrotic area at the crush site, some undergoing division (Fig. 7c). At higher magnification, elongated mpcs (expressing MRFs; not shown here) were observed to

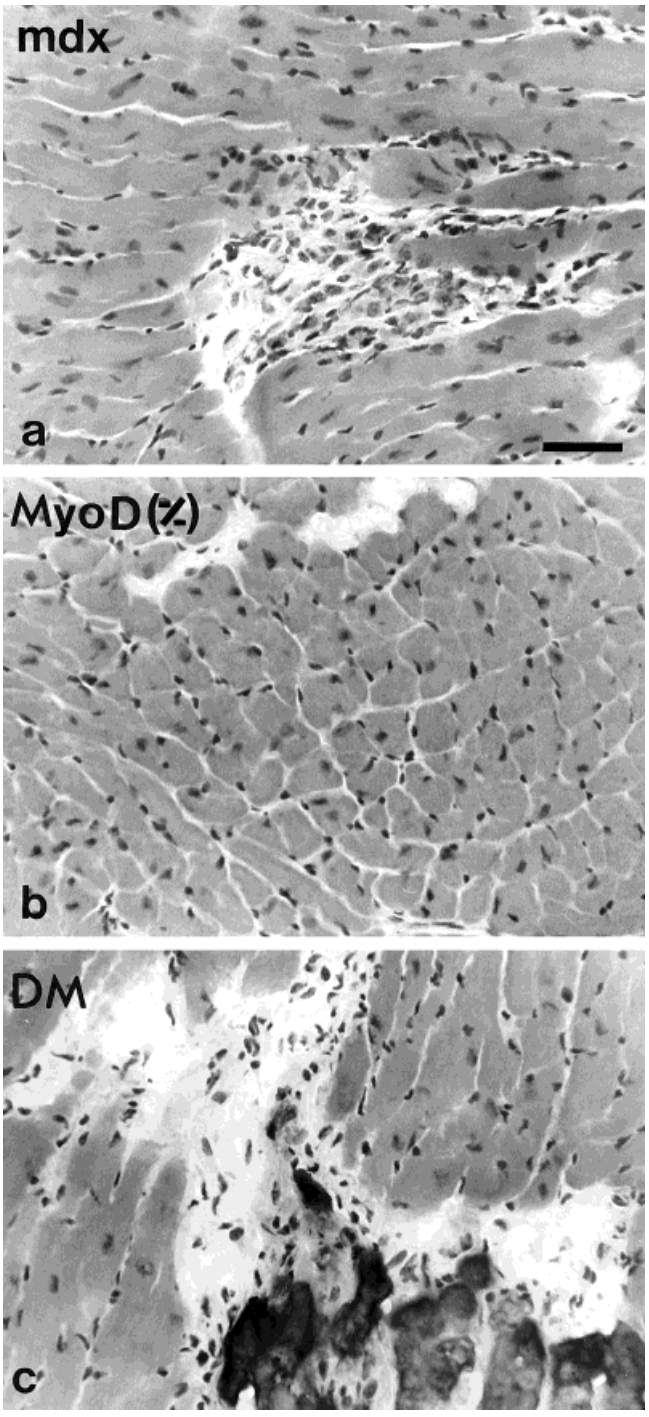

Fig. 6. Cardiac muscle from *mdx*(a), MyoD(-/-) (b), and double-mutant (c) mice (magnification ×240). **a:** In *mdx* cardiac muscle, small foci of circumscribed cardiomyocyte necrosis and mononuclear cell infiltration are present in both ventricles and, to a lesser extent, in the atria. **b:** MyoD(-/-) cardiac muscle shows a normal morphology in which myocytes contain central nuclei, and no lesions are present. **c:** In double-mutant hearts, dystrophic lesions are very large and very often contain large amounts of calcified tissue within pockets of mononuclear cell infiltration. Lesions are present in papillary, subendocardial, and subepicardial regions of double-mutant hearts. Scale bar = 50 μm.

be misaligned (not parallel to the long axis of the muscle; Fig. 7d). Double-mutant RTAs contained substantially more myotubes than in MyoD(-/-) RTAs (compare Fig. 7e with Fig. 7c), whereas double-mutant myotubes were fewer and smaller than in *mdx* RTAs (compare Fig. 7e with Fig. 7a). Mpcs and mononuclear cells were numerous between myotubes and were often large and elongated toward the ends of surviving fibers, as seen in *mdx* RTAs (compare Fig. 7f with 7b). Therefore, new myotube formation was greatest in *mdx* RTA muscles, lowest in MyoD(-/-) muscles, and intermediate in double-mutant regenerating muscles.

After in situ hybridization studies, myogenic cells expressing mRNA transcribed from either myf5 or myogenin genes were labeled by red-brown staining in the sarcoplasm of new myotubes and mononuclear cells in the RTA and DIA muscles from all three strains. MRF+ cells were also present in regenerating dystrophic foci of *mdx* and double-mutant LTAs, whereas the MyoD(-/-) LTAs contained very rare MRF+ cells. Autoradiograms demonstrated proliferating cells in regenerating muscles and in dystrophic muscles that did not receive a crush injury. Regardless of cell type, many mononuclear cells in crush-injured *mdx* (Figs. 8a–d, 9a–-c), MyoD(-/-) (Figs. 8e–g, 9d–g), and double-mutant (Figs. 8h–k, 9h–l) mice contained a nucleus that was labeled with silver grains.

In MyoD(-/-) RTA, myotubes were fewer, shorter, narrower, and contained fewer nuclei compared with *mdx* RTA. These features of myotubes in double-mutant RTA were intermediate compared with MyoD(-/-) or *mdx* RTA. In addition, there were many nuclei labeled by silver grains in myotubes of *mdx* RTA compared with the RTAs of the other two strains (Figs. 8c,g, 9c,l). There were virtually no myotube nuclei labeled by silver grains in MyoD(-/-) RTA muscles. Therefore, the extent of new myotube formation in regenerating muscles was greatest in the *mdx* RTA muscles, least in MyoD(-/-) RTA muscles, and intermediate in the RTA muscles of double-mutant mice. Large numbers of mononuclear cells were found adjacent to the necrotic crushed area in MyoD(-/-) muscles, suggesting that inflammation and phagocytosis were delayed in MyoD(-/-) RTA compared with *mdx* RTA. Therefore, systematic observations of regenerating muscle samples from three strains confirm that the absence of MyoD expression results in reduced regeneration and fusion and a decreased rate of DNA synthesis by muscle precursors, as marked by incorporated isotope in myotube nuclei.

The tandem use of in situ hybridization and autoradiography allowed identification of myogenic cells and determination of the proliferative proportions of myf5+ and myogenin+ precursors present in regenerating muscle. There were many more proliferating mononuclear cells that were not myogenic (i.e., that did not contain myf5 or myogenin mRNA) in MyoD(-/-) RTA than in the RTA muscle of the other two strains (Figs. 8, 9), in agreement with earlier findings (Megeney et al., 1996). In general, there were fewer proliferative myogenic cells that were positive for the myf5 signal than for the myogenin in situ staining, and there were many more proliferating MRF+ cells in RTAs of *mdx* mice than in either of the strains that lacked MyoD. This was observed for both myf5+ muscle precursors (compare Fig. 8a–d with Fig. 8e–g and Fig. 8h–k) and myogenin+ muscle precursors (compare Fig. 9a–c with Fig. 9d–g and Fig. 9h–l).

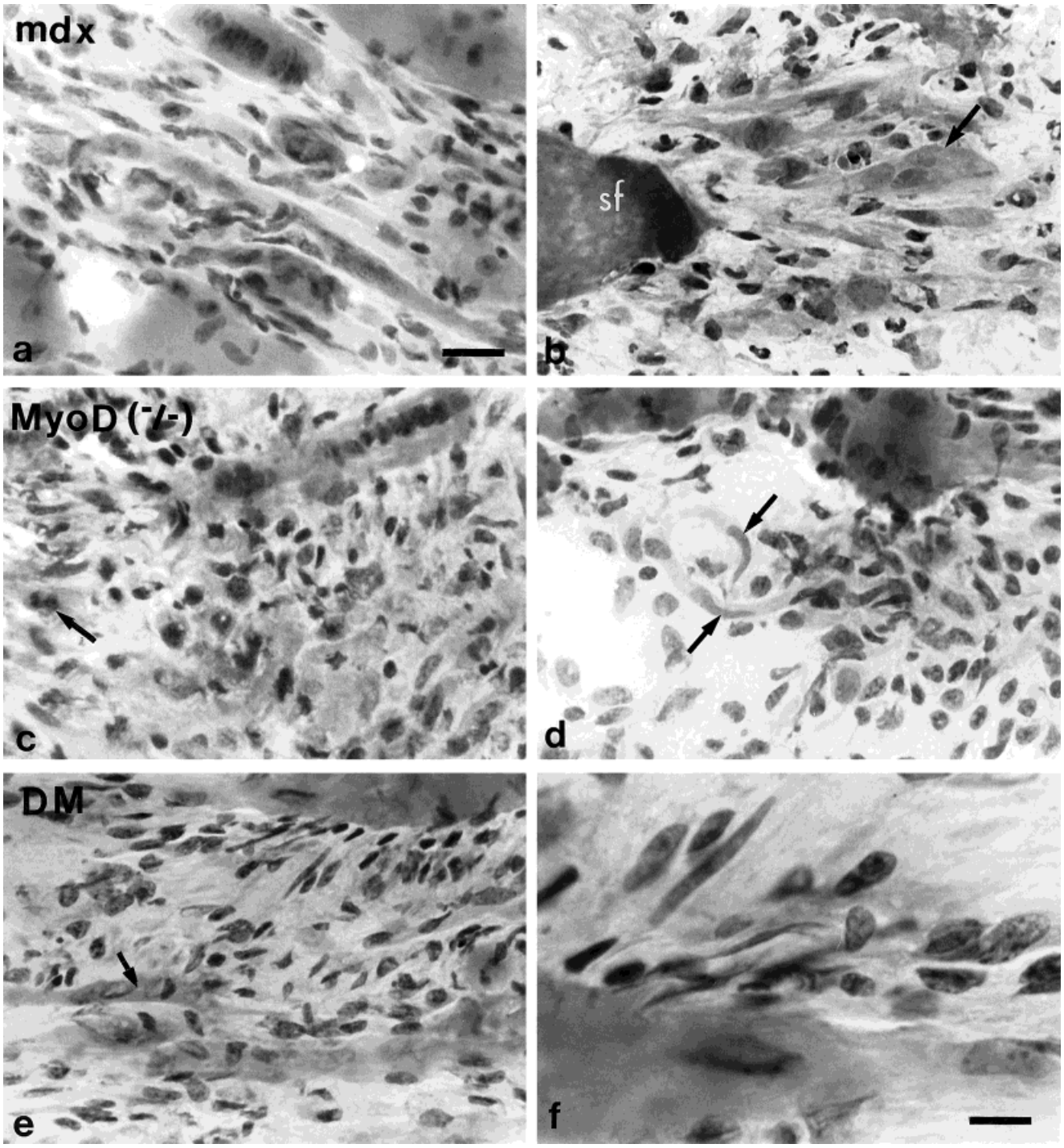

Fig. 7. Regenerating tibialis anterior muscles 4 days after injury to *mdx*(a,b), MyoD(-/-) (c,d), and double-mutant (e,f) mice. **a:** In *mdx* muscle, there are mononuclear cells between the many new myotubes arranged longitudinally and formed de novo from fused myoblasts (magnification ×450 in a–e). **b:** Numerous cells with one to three nuclei are present near the end of this surviving fiber (sf) and appear to be migrating toward or away from the fiber due to their radial arrangement with the fiber. **c:** In MyoD(-/-) muscle, there are visible mitotic figures (arrow), very few myotubes, and many mononuclear cells present in the regenerating muscle. **d:** At high magnification, elongated myocytes (arrows) are misaligned compared with the radial arrangement observed in b, and relatively few appear close to surviving fiber segments. **e:** In double-mutant regenerating muscle, elongated myotubes are present and are surrounded by numerous mononuclear cells. **f:** The pattern of angulated mononuclear cells juxtaposed to surviving fiber segments is observed and is similar to that in *mdx* regenerating muscle (magnification ×1,120). Scale bars = 25 μm in a (also applies to b–e), 10 μm in f.

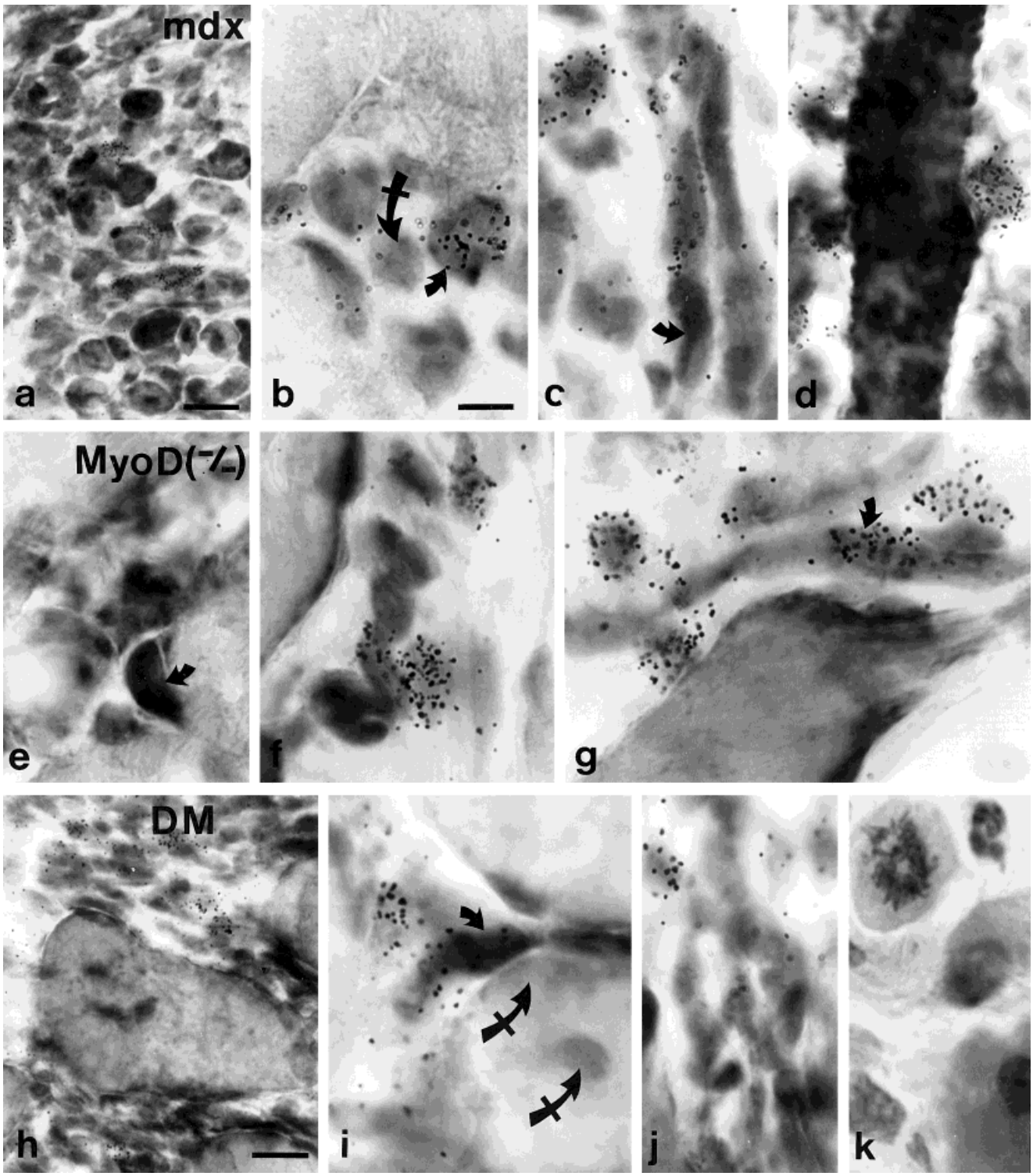

Fig. 8.

Data on proliferation by myf5+ and myogenin+ mononuclear cells in the RTAs of the three strains (Table 2) show that myogenic cell proliferation was greatest in *mdx* RTA muscles (18% of myf5+ cells; 30% of myogenin+ cells). In marked contrast, MyoD(-/-) RTAs contained virtually no proliferative myf5+ or myogenin+ cells. Although there were essentially no proliferative myf5+ cells in the double-mutant RTA, 12% of myogenin+ precursors were proliferating in double-mutant RTA muscles, intermediate between levels in *mdx* and MyoD(-/-) RTA. Thus, myo-

genin+ precursors are twofold more proliferative than myf5+ precursors in vivo in adult *mdx* myogenesis, whereas myf5+ precursors do not proliferate in the absence of MyoD. Proliferation of myogenin+ precursors in *mdx* muscle regeneration is nearly twice that in double mutants, and, again, myogenin+ precursors that lack MyoD expression do not proliferate.

DISCUSSION

The current series of experiments coupled proton NMR spectroscopy and molecular biology to address whether the pattern of muscle regeneration is correlated with the levels of myogenic cell proliferation and differentiation and taurine biochemistry. First, in combination with new, detailed histologic studies of myopathy and muscle regeneration, we report that taurine (and carnitine) levels are reduced during dystrophy-induced damage, rise in tandem with greater regeneration, and change consistently in muscle NMR samples ex vivo and in extracts. The increases in taurine with greater regeneration occur independent of the muscle type or genetic etiology of the fiber damage. The application of comparisons among four different strains (with or without MyoD and/or dystrophin expression) and different muscle phenotypes suggests that the metabolic changes are more likely to be significant indicators of muscle status than particular phenomena of *mdx* muscles. Also, these data show that early proliferation of myogenic cells after injury and prior to fusion bears a strong prognostic relation to the outcome of skeletal muscle regeneration. In combination, the two perspectives suggest the intriguing possibility that ^{1}H-NMR could detect shifts in taurine and other metabolites that mark the directional shifts between muscle disease, damage, and regeneration in correlation with myogenic proliferation.

Perchloric acid extracts of muscle provided strong data that *mdx* muscles exhibit alterations in energy metabolism during dystrophy, including shifts in carnitine, alanine, glutamate, and succinate in different muscles. The physiological significance of the change in taurine is not known, although it may be a consequence of myofiber degeneration and necrosis, prominent at 5 weeks of age (Dangain and Vrbova, 1984; Anderson et al., 1987). Alternatively, reduced taurine may contribute to segmental fiber damage secondary to the lack of dystrophin. Reports that taurine plays a role in cell proliferation and viability (Wright et al., 1986; Huxtable, 1992) further suggest that taurine in muscle could be depleted by the proliferation of muscle precursors and an early burst of regeneration, which is also active around 5 weeks in *mdx* dystrophy (Anderson et al., 1987; McGeachie et al., 1993). The lower than normal muscle carnitine level (Nakajima et al., 1994) detected in *mdx* TA is in agreement with earlier DMD studies using other techniques (Berthillier et al., 1982; Camina et al., 1995). Carnitine may be lost through membrane breaches during dystrophy, because necrotic fibers are not observed in primary carnitine myopathies (Rebouche and Engel, 1984). The alternative explanation, that carnitine content relates to muscle fiber regeneration, is supported by two findings. Carnitine is decreased in rat muscle regeneration induced by bupivacaine (Czyzewski et al., 1983), and *mdx* dystrophic muscles show a burst of repair at 5 weeks.

Additional metabolites were altered in *mdx* diaphragm but not in the TA muscle, and this likely was due to the greater involvement of the diaphragm in dystrophy. Lower levels of alanine, glutamate, and succinate in *mdx* compared with normal diaphragm extracts may be further demonstration of decreased oxidative use of glucose and free fatty acids during damage (Decrouy et al., 1993; Even et al., 1994; Mokhatarian and Even, 1996) or secondary to the decreased muscle:nonmuscle mass in the *mdx* diaphragm (Stedman et al., 1991; Anderson et al., 1998).

Our detailed study of regeneration, using in situ hybridization and autoradiography coupled with ^{1}H-NMR of *mdx*, MyoD(-/-) and double-mutant (*mdx*:MyoD-/-) muscles showed that the changes in metabolites are entirely consistent from extracts to ex vivo (biopsy) samples, that taurine and carnitine were reproducibly high in muscles with effective regeneration, and that spectroscopy data for those moieties correlate with proliferation by late muscle precursors (expressing myogenin), whereas others show the inverse relation (lipid, lactate). If ^{1}H-NMR changes are due to specific key proliferation and differentiation events underlying regeneration, and if the consistent findings in resonant moieties are based on phenotypes of disease, muscle type, and the extent of regeneration, then there is a substantial potential for ^{1}H-NMR monitoring of muscle status in disease, repair, and treatment. The counterpart evidence that myogenic cell proliferation parallels both ^{1}H-NMR findings and muscle phenotypes further suggests that there are specific changes in the biochemistry of myogenesis that reflect phenotypic and possibly genotypic alterations. In particular, the apparent inhibition in MyoD-deficient muscles of proliferation by myf5-positive muscle precursors was distinct from the buffered proliferation by

Fig. 8. Examples of tandem in situ hybridization for myf5 expression and autoradiography of ^{3}H-thymidine incorporation into proliferating cells in *mdx* (**a–d**), MyoD(-/-) (**e–g**), and double-mutant (**h–k**) right (crushed) TA (RTA) muscles. Two low-magnification views of regenerating *mdx* (a) and double-mutant (h) muscle containing proliferative and nonproliferative cells plus in situ staining for myf5 mRNA are shown for orientation. The very dark in situ alkaline-phosphatase staining is confined to the cytoplasm, and nuclei are lightly counterstained with hematoxylin, which is distinctive in color from the in situ signal. Although the grains of the in situ stain are in focus, not all grains are in a single focal plane, because the autoradiography emulsion has depth on the section. The in situ staining appears in mononuclear cells (e.g., at small arrow in b), in cells at the satellite position on remnant fibers (e.g., at arrow in e), and in the sarcoplasm of new myotubes (e.g., at arrow in c, at small arrow in i). The very few new myotubes that are present in MyoD(-/-) RTAs are not always stained by in situ hybridization for myf5 mRNA (g). The myf5 in situ signal is also present in sarcoplasm of short surviving segments that are surrounded by both MRF-positive and MRF-negative mononuclear cells (d). By comparison, myf5-negative nuclei in muscle fibers (including myonuclei and putative satellite cell nuclei that are not expressing MRF mRNA) and in mononuclear cells are stained only lightly by hematoxylin and are not surrounded by a dense in situ signal (e.g., at crossed arrows in b and i). Nuclei labeled with silver grains are present in the satellite cell position on remnant fibers and among mononuclear cells (c,g), including those angulated from surviving segments (d). Proliferative nuclei are also found within myotubes (c,g,i). Proliferative myf5-positive myogenic cells are present in *mdx* (a–d) and double-mutant RTA muscle (h–k). One of the proliferative monouclear cells extending to/from an myf5-positive segment is observed to be proliferative (d). Myf5-positive proliferating cells are very infrequent and are absent more often from MyoD(-/-) RTA muscles (e–g) despite the presence of many large cells observed in mitosis, as observed in hematoxylin and eosin (H&E)-stained sections of the same muscles (k). Magnification ×400 in a and h, ×990 in b–g and i–k. Scale bars = 25 μm in a and h, 10 μm in b (also applies to c–g and i–k).

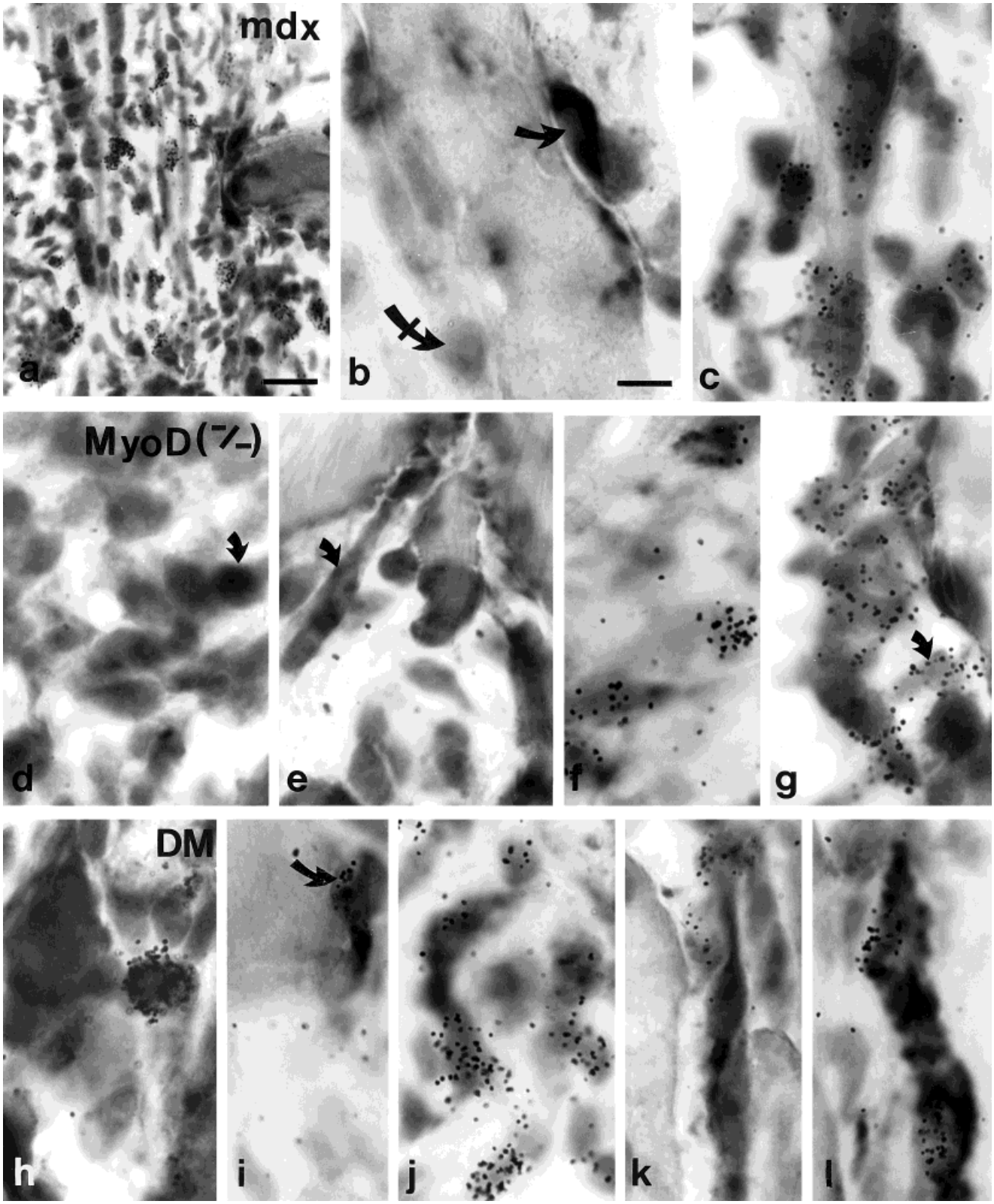

Fig. 9.

TABLE 2. Total Number and Proliferative Proportion (%) of Mononuclear Myogenic Cells (myf5$^+$ or Myogenin$^+$) Observed in Six Fields of Each Right (Crushed) Tibialis Anterior Muscle in *mdx* Mice (n = 2), MyoD(−/−) Mice (n = 3), and *mdx*:MyoD(−/−) Double-Mutant Mice (n = 5)[a]

	Myf5$^+$ mpcs		Myogenin$^+$ mpcs	
Mice	Total number	Proliferative proportion (%)	Total number	Proliferative proportion (%)
mdx	343	18	355	32
	84	—	316	28
MyoD(−/−)	193	3	278	0
	—	—	338	0
	85	0	209	0
mdx:MyoD(−/−)	389	0	350	12
	—	—	103	14
	137	0	393	7
	37	0	229	13
	60	8	428	13
Mean ± SEM		2 ± 4[b]		12 ± 3[b,c]

[a]Myogenic cells were identified by using in situ hybridization, and, in combination with autoradiography, the proliferative proportions of the two cell populations were identified. Dash (—) indicates that either in situ hybridization or autoradiography procedures were not adequate for observations (counting from six fields).
[b]Significantly different from the *mdx* group.
[c]Significantly different from the proliferative proportion of myf5$^+$ muscle precursors (mpcs) in the same group and from the MyoD(−/−) group.

later, more differentiated myogenin-positive precursors in double-mutant muscle regeneration. Studies are now in progress to investigate further the time-course of ^{1}H-NMR changes during regeneration, the potential application of magnetic resonance imaging to monitor phenotypic disease changes (e.g. *mdx* dystrophy; McIntosh et al., 1998b and regulation of precursor amplification after satellite cell activation.

The mechanisms that allow genotype to modulate proliferation by muscle precursors expressing myogenin but not myf5 are not known but are likely to implicate oncogene, growth, and scatter factor effects on cell cycling and commitment. For example, there is a switch between c-met receptor expression by quiescent satellite cells (Cornelison and Wold, 1998) and expression of both c-met and its ligand scatter factor (hepatocyte growth factor) by activated muscle precursors in vitro and in vivo (Tatsumi et al., 1998). That switch in expression overlaps the period when satellite cells enter the cell cycle and express muscle regulatory genes (Yablonka-Reuveni and Rivera, 1994; Anderson, unpublished observations). We suggest that the same period of early regeneration may be identifiable clinically by using ^{1}H-NMR to examine changes in taurine and oxidative metabolism in vivo.

Fig. 9. Examples of tandem in situ hybridization for myogenin expression and autoradiography for proliferating cells labeled with silver grains exposed by ^{3}H-thymidine incorporation in *mdx* (a–c), MyoD(-/-) (d–g) and double-mutant (h–l) RTA muscles. A low-magnification view of regenerating *mdx* muscle is shown (a). The in situ staining for myogenin is similar to that for myf5 and is confined to the cytoplasm of mononuclear cells in regenerating muscle (c–e,h,j), in cells at the satellite cell position on surviving fibers (e.g., at small arrow in b, at arrow in i), and in the sarcoplasm of new myotubes (c,e,k,l). By comparison, myogenin-negative nuclei that are not surrounded by the dense in situ signal are stained only lightly by hematoxylin (e.g., at crossed arrow in b). Nuclei labeled with silver grains are present in the satellite cell position on remnant fibers (i), among mononuclear cells (a,f,h,j), and within myotubes (c,l). Proliferative myogenin-positive myogenic cells are present in *mdx* (a,c) and double-mutant (h,j,l) RTA muscle. Proliferative myogenin-positive cells are also present in MyoD(-/-) RTA muscles (d–g), although most myogenin-positive mononuclear cells are not proliferative (d–f).A proliferative myogenin-positive satellite cell is shown in a double-mutant RTA (i). Magnification ×400 in a, ×990 in b–l. Scale bars = 25 μm in a, 10 μm in b (also applies to c–l).

ACKNOWLEDGMENTS

Spectra were acquired at the Prairie Regional NMR Facility, University of Manitoba, with the assistance of T. Wolowiec. We thank M. Donnelly and C. Vargas for assisting in the extraction procedure and tissue sectioning and R. Simpson for technical expertise. This work was supported by grants from the Children's Hospital Research Foundation and the Muscular Dystrophy Association to J.E.A. and by the Medical Research Council of Canada, the Muscular Dystrophy Association, and the National Cancer Institute (M.A.R.). A postdoctoral fellowship from MRC/MDA (K.L.G) and a Ph.D. studentship from MRC (L.M.M.) also supported this work.

LITERATURE CITED

Anderson JE, Ovalle WK, Bressler BH. Electron microscopic and autoradiographic characterization of hindlimb muscle regeneration in the *mdx* mouse. Anat. Rec. 1987;219:243–257.

Anderson JE, Bressler BH, Ovalle WK. Functional regeneration in the hindlimb skeletal muscle of the *mdx* mouse. J. Muscle Res. Cell Motil. 1988;9:499–516.

Anderson JE, Garrett K, Moor A, McIntosh L, Penner K. Dystrophy and myogenesis in *mdx* diaphragm muscle. Muscle Nerve 1998;21 (in press).

Arus C, Barany M. Application of high-field ^{1}H-NMR spectroscopy for the study of perifused amphibian and excised mammalian muscles. Biochim. Biophys. Acta 1986;886:411–424.

Berthillier G, Eichenberger D, Carrier HN, Guibaud P, Got R. Carnitine metabolism in early stages of DMD. Clin. Chim. Acta 1982;122: 369–375.

Camina F, Novo-Rodriguez MI, Rodriguez-Segade S, Castro-Gago M.

Purine and carnitine metabolism in muscle of patients with Duchenne muscular dystrophy. Clin. Chim. Acta 1995;243:151–164.
Cornelison DD, Wold BJ. Single-cell analysis of regulatory gene expression in quiescent and activated mouse skeletal muscle. Dev. Biol. 1998;191:270–283.
Czyzewski K, Stern LZ, Sadeh M, Bahl JJ. Changes in muscle carnitine during regeneration. Ann. Neurol. 1983;14:126.
Dangain J Vrbova G. Muscle development in *mdx* mutant mice. Muscle Nerve 1984;7:700–704.
Decrouy A, Even PC, Chinet A. Decreased rates of Ca^{2}+-dependent heat production in slow- and fast-twitch muscle from dystrophic (*mdx*) mouse. Experientia 1993;49:843–849.
Dupont-Versteegden EE, McCarter RJ. Differential expression of muscular dystrophy in diaphragm versus hindlimb muscles of *mdx* mice. Muscle Nerve 1992;15:1105–1110.
Even PC, Decrouy A, Chinet A. Defective regulation of energy metabolism in *mdx*-mouse skeletal muscle. Biochem. J. 1994;304:649–654.
Garrett KL, Anderson JE. Colocalization of bFGF and the myogenic regulatory gene myogenin in dytrophic *mdx* muscle precursors and young myotubes in vivo. Dev. Biol. 1995;169:596–606.
Huxtable RJ. Physiological actions of taurine. Physiol. Rev. 1992;72: 101–163.
Kuesel AC, Kroft T, Saunders JK, Prefontaine M, Mikhael N, Smith ICP. A simple procedure for obtaining high-quality NMR spectra of semiquantitative value from small tissue specimens: Cervical biopsies. Magn. Reson. Med. 1992;27:349–355.
Kuesel AC, Donnelly SM, Halliday W, Sutherland GR, Smith ICP. Mobile lipids and metabolic heterogeneity of brain tumors as detectable by ex vivo ^{1}H MR spectroscopy. N.M.R. Biomed. 1994;7: 172–180.
Matsumura K, Campbell KP. Dystrophin-glycoprotein complex: Its role in the molecular pathogenesis of muscular dystrophies. Muscle Nerve 1994;17:2–15.
McGeachie JK, Grounds MD, Partridge TA, Morgan JE. Age-related changes in replication of myogenic cells in *mdx* mice: Quantitative autoradiographic studies. J. Neurol. Sci. 1993;119:169–170.
McIntosh LM, Anderson JE. Hypothyroidism prolongs and increases mdx muscle precursor proliferation and delays myotube formation in normal and dystrophic limb muscle. Biochem. Cell Biol. 1995;73: 181–190.
McIntosh LM, Pernitksy AP, Anderson JE. The effects of altered metabolism (hypothyroidism) on muscle repair in the *mdx* dystrophic mouse. Muscle Nerve 1994;17:444–453.
McIntosh LM, Granberg KE, Briere KM, Anderson JE. A nuclear magnetic resonance spectroscopy study of muscle growth, *mdx* dystrophy and glucocorticoid treatments: Correlation with repair. N.M.R. Biomed. 1998;11:1–10.
McIntosh LM, Baker RE, Anderson JE. Magnetic resonance imaging of regenerating and dystrophic mouse muscle. Biochem. Cell Biol. 1998b (in press).
Megeney L, Rudnicki MA. Determination versus differentiation and the MyoD family of transcription factors. Biochem. Cell Biol. 1995;73:723–732.
Megeney LA, Kablar B, Garrett K, Anderson JE, Rudnicki MA. MyoD is required for myogenic stem cell function in adult skeletal muscle. Genes Dev. 1996;10:1173–1183.
Mizuno Y, Yoshida M, Nonaka I, Hirai S, Ozawa E. Expression of utrophin (dystrophin-related protein) and dystrophin-associated glycoproteins in muscles from patients with Duchenne muscular dystrophy. Muscle Nerve 1994;17:206–216.
Mokhatarian A, Even PC. Effect of intraperitoneal injection of glucose on glucose oxidation and energy expenditure in the mdx mouse model of Duchenne muscular dystrophy. Pfluger's Arch. 1996;432: 379–385.
Moreno A, Arus C. Quantitative and qualitative characterization of 1-H NMR spectra of colon tumors, normal mucosa and their perchloric acid extracts: Decreased levels of myo-inositol in tumors can be detected in intact biopsies. N.M.R. Biomed. 1996;8:33–45.
Nakajima H, Sugie H, Tsurui S, Ito M. Application of 1-H NMR spectroscopy for qualitative measurement of muscle carnitine levels. Clin. Chim. Acta 1994;224:81–88.
Peeling J, Sutherland G. High resolution ^{1}H-NMR spectroscopy studies of extracts of human cerebral neoplasms. Magn. Reson. Med. 1992;24:123–136.
Peeling J, Sutherland G. 1-H magnetic resonance spectroscopy of extracts of human epileptic neocortex and hippocampus. Neurology 1993;43:589–594.
Pernitsky AP, McIntosh LM, Anderson JE. Hyperthyroidism impairs early repair in normal but not dystrophic *mdx* mouse tibialis anterior muscle: An in vivo study. Biochem. Cell Biol. 1996;74:315–324.
Rebouche CJ, Engel AG. Kinetic compartmental analysis of carnitine metabolism in the human carnitine deficiency syndromes: Evidence for alterations in tissue carnitine transport. J. Clin. Invest. 1984;73: 857–867.
Rudnicki MA, Jaenisch R. The MyoD family of transcription factors and skeletal myogenesis. Bioessays 1995;17:203–209.
Rudnicki MA, Braun T, Hinuma S, Jaenisch R. Inactivation of MyoD in mice leads to upregulation of the myogenic HLH gene Myf-5 and results in apparently normal muscle development. Cell 1992;71:383–390.
Rutter A, Hugenholtz H, Saunders J, Smith ICP. Classification of brain tumors by ex vivo ^{1}H NMR spectroscopy. J. Neurochem. 1995;64:1655–1661.
Stedman HH, Sweeney HL, Schrager JB, Maguire HC, Panettieri RA, Petrof B, Narusawa M, Leferovich JM, Sladky JT, Kelly AM. The *mdx* mouse diaphragm reproduces the degenerative changes of Duchenne muscular dystrophy. Nature 1991;352:536–538.
Sze DY, Jardetzky O. Determination of metabolite and nucleotide concentrations in proliferating lymphocytes by ^{1}H-NMR of acid extracts. Biochim. Biophys. Acta 1990;1054:181–197.
Sze DY, Jardetzky O. High-resolution proton NMR studies of lymphocyte extracts. Immunomethods 1994;4:113–126.
Tatsumi R, Anderson JE, Nevoret CJ, Halevy O, Allen RE. HGF/SF is present in normal and adult skeletal muscle and is capable of activating satellite cells. Dev. Biol. 1998;194:114–128.
Venkatasubramanian PN, Arus C, Barany M. Two-dimensional proton magnetic resonance of human muscle extracts. Clin. Physiol. Biochem. 1986;4:285–292.
Weintraub H, Davis R, Tapscott S, Thayer M, Krause M, Benezra B, Blackwell TK, Turner D, Rupp H, Hollenberg S, Zhuany Y, Lasser AB. The MyoD gene family: Nodal point during specification of the muscle cell lineage. Science 1991;251:761–766.
Wright CE, Tallan HH, Yong YL. Taurine: Biological update. Annu. Rev. Biochem. 1986;55:427–453.
Yablonka-Reuveni Z, Rivera AJ. Temporal expression of regulatory and structural muscle proteins during myogenesis of satellite cells on isolated adult rat fibers. Dev. Biol. 1994;164:588–603.